

Mesoscopic Simulations of Electroosmotic Flow and Electrophoresis in Nanochannels

Jens Smiatek^a, Friederike Schmid^b

^a*Institut für Physikalische Chemie, Universität Münster, Germany*

^b*Institut für Physik, Universität Bielefeld, Germany*

Abstract

We review recent dissipative particle dynamics (DPD) simulations of electrolyte flow in nanochannels. A method is presented by which the slip length δ_B at the channel boundaries can be tuned systematically from negative to infinity by introducing suitably adjusted wall-fluid friction forces. Using this method, we study electroosmotic flow (EOF) in nanochannels for varying surface slip conditions and fluids of different ionic strength. Analytic expressions for the flow profiles are derived from the Stokes equation, which are in good agreement with the numerical results. Finally, we investigate the influence of EOF on the effective mobility of polyelectrolytes in nanochannels. The relevant quantity characterizing the effect of slippage is found to be the dimensionless quantity $\kappa\delta_B$, where $1/\kappa$ is an effective electrostatic screening length at the channel boundaries.

Keywords: Dissipative Particle Dynamics; slip length; electrolytes; electroosmotic flow; electrophoresis; microfluidics

1. Introduction

Microfluidic devices like bio-MEMS (micro-electronical-mechanical-systems) and bio-NEMS (nano-electronical-mechanical-systems) are attracting growing interest due to their huge potential in bio- and nanotechnology, *e.g.*, for analyzing and manipulating tiny samples. Due to the large surface-to-volume ratios in nanoconfined systems, the flow in such devices is strongly influenced by the specific properties of the boundaries, *i.e.*, by surface characteristics like the wetting behavior and/or slippage.

If electric fields are involved, one particularly important mechanism is electroosmotic transport: In contact with a liquid, many materials commonly used in nanotechnology (*e.g.*, polydimethylsiloxane (PDMS)) acquire surface charges due to the ionization of surface groups [1]. Surfaces are thus often covered by a compensating counterion layer [2]. If one applies an external electric field, the ions are driven in one direction and drag the surrounding fluid along, thus creating the so-called electroosmotic flow (EOF). This electrokinetic effect has numerous consequences: It alters drastically the migration dynamics of mesoscopic objects like

polyelectrolytes or colloids [3]. In microchannels, the EOF generated at the channel walls induces a total net flow, which is technologically attractive because it can be controlled and manipulated more easily on the sub-micrometer scale than pressure- or shear-driven flow.

One important application of microchannels is to use them for separating different fragments of biological molecules like DNA by their length for sequencing or further manipulation. In free solution, the electrophoretic mobility of high molecular weight polyelectrolytes is length independent [3]. Electrophoretic separation methods therefore often introduce the samples into micro- or nanostructured environments, *e.g.*, disordered gels (in gel electrophoresis), or structured microchannels [3, 4, 5, 6, 7, 8, 9, 10, 11, 12, 13]. The migration behavior of the molecules in such a setup results from a complex interplay of electrostatics, hydrodynamics, and confinement effects on the molecules, and modeling all of this in full detail is computationally challenging. Fortunately, it turns out that due to a combination of subtle screening effects – which are not yet fully understood – simple implicit-solvent Brownian Dynamics simulations that altogether neglect electrostatic and hydrodynamic interactions give results that are in qualitative and semiquantitative agreement with experiments [3, 14, 15]. Nevertheless, such simplified

Email address: e-mail:

Friederike.Schmid@Uni-Mainz.DE (Friederike Schmid)

treatments miss important and interesting physics, and simulations with explicit solvent and explicit charges are clearly desirable.

Here we present such explicit simulations of EOF and polyelectrolyte electrophoresis in nanochannels [16, 17], using Dissipative Particle Dynamics (DPD) [18, 19], which is a popular mesoscopic simulation method. Particular emphasis is put on the role of the channel boundaries, *i.e.*, on the effect of slippage and the electrical double layer at the surface.

The remainder of the paper is organized as follows: After some theoretical considerations, we describe the simulation model and method, with special focus on our method to implement variable hydrodynamic boundaries. Then we discuss the results, first for the simpler situation of a charged channel which only contains counterions, and finally for the full problem (electrolyte of varying ionic strength plus polyelectrolyte plus counterions). The results are compared with theory wherever possible. We conclude with a brief summary.

2. Theoretical considerations: EOF in slit channels

We consider a planar slit channel with identical walls at $z = \pm L/2$, exposed to an external electric field E_x in the x direction. The electrostatic potential Φ then takes the general form $\Phi(x, y, z) = \psi(z) + E_x x + \text{const}$, where we can set $\psi(0) = 0$ for simplicity. Comparing the Poisson equation for the electrostatic potential ψ with the Stokes equation and exploiting the symmetry of the channel, one finds [17]

$$v_x(z) = \psi(z) \cdot \epsilon_r E_x / \eta_s + v_{\text{EOF}}, \quad (1)$$

where ϵ_r is the dielectric constant, η_s the shear viscosity of the fluid, and $v_{\text{EOF}} = v_x(0)$ is an integration constant.

On the nanoscale, the appropriate hydrodynamic boundary condition at the channel walls is the partial-slip boundary condition

$$\delta_B \partial_z v(x)|_{z_B} = v_x(z)|_{z_B}, \quad (2)$$

where $v_x(z)$ denotes the component of the velocity in x -direction evaluated at the position z_B of an effective ‘‘hydrodynamic boundary’’ position, and the second effective parameter, the slip length δ_B , characterizes the amount of slippage at the surface. Inserting Eq. (2) into Eq. (1), we finally obtain the following simple expression for the electroosmotic mobility,

$$\mu_{\text{EOF}} = v_{\text{EOF}} / E_x = \mu_{\text{EOF}}^0 (1 + \kappa \delta_B), \quad (3)$$

where we have defined an inverse ‘surface screening length’ [17]

$$\kappa := \mp \partial_z \psi / \psi|_{z=\pm z_B}, \quad (4)$$

and μ_{EOF}^0 is the well-known Smoluchowski result [2] for the electroosmotic mobility at sticky walls $\mu_{\text{EOF}}^0 = -\epsilon_r \psi(z_B) / \eta_s$. A similar result can be derived within the linearized Debye-Hückel theory with $\kappa = \kappa_D$ (the Debye-Hückel length) [20].

3. Simulation Method

We study fluids that are driven through planar slit channels in the x -direction by external fields, applying periodic boundaries in the x and y dimension and repulsive (charged) walls in the z direction. The systems contained varying amounts of charged ions (anions and cations), plus possibly a polyelectrolyte chain. They were thermalized by the momentum conserving DPD thermostat [18, 19], where the forces acting on particles i are given by a sum $\vec{F}_i^{\text{DPD}} = \vec{F}_i^{\text{C}} + \sum_{j \neq i} (\vec{F}_{ij}^{\text{D}} + \vec{F}_{ij}^{\text{R}})$ of standard conservative contributions \vec{F}_i^{C} , dissipative forces \vec{F}_{ij}^{D} , and random forces \vec{F}_{ij}^{R} with

$$\vec{F}_{ij}^{\text{D}} = -\gamma_{\text{DPD}} \omega(r_{ij}) (\hat{r}_{ij} \cdot \vec{v}_{ij}) \hat{r}_{ij} \quad (5)$$

$$\vec{F}_{ij}^{\text{R}} = \sqrt{2 \gamma_{\text{DPD}} k_B T \omega(r_{ij})} \check{\zeta}_{ij} \hat{r}_{ij}. \quad (6)$$

Here $\omega(r)$ is an arbitrary weight function with finite range r_c (chosen linear in our case, $\omega(r) = 1 - r/r_c$ for $r < r_c$), γ_{DPD} is a friction coefficient, $\hat{r}_{ij} = \vec{r}_{ij}/r_{ij}$ the unit vector in the direction of particle j , T the temperature, k_B the Boltzmann factor, and $\check{\zeta}_{ij} = \check{\zeta}_{ji}$ are uncorrelated Gaussian distributed random variables with zero mean and unit variance. In DPD simulations, the conservative forces are often taken to have a certain soft shape. Here we only use the DPD *thermostat* as described above. All simulations have been carried out with extensions of the freely available software package ESPResSo [21].

3.1. Simulation Model

All particles, solvent, ions, and chain monomers, are modeled explicitly, and have the same mass m for simplicity. Ions and monomers repel each other with a soft repulsive Weeks-Chandler-Anderson (WCA) potential [22] of range σ and amplitude ϵ . The same potential acts between particles and the walls. In addition, chain monomers are connected by harmonic springs $U_{\text{harmonic}} = \frac{1}{2} k (r_{ij} - r_0)^2$ with the spring constant $k = 25\epsilon/\sigma^2$ and $r_0 = 1.0\sigma$. Neutral solvent particles have no conservative interactions except with the walls. The wall contains immobilized, negatively charged particles at random positions. Every second monomer on the polyelectrolyte carries a negative charge. All charges

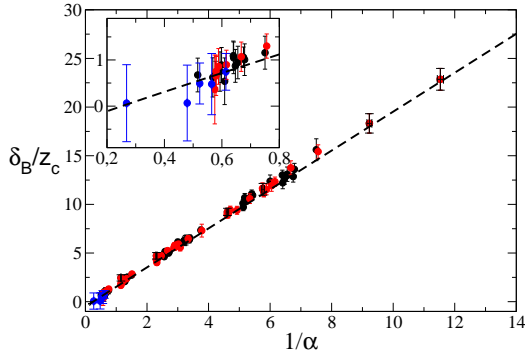


Figure 1: Slip length δ_B in units of z_c vs. α for varying values of the parameter triplet $(\rho, \gamma_{DPD}, \gamma_L)$ (in units of σ^{-3} or $\sqrt{m\epsilon}/\sigma$, respectively). Black: series with ρ fixed: (3.75, 2-10, 0.1-1). Red: series with γ_{DPD} fixed: (3.75-12.5, 2, 0.1-1). Blue: selected triplet values: (6.35, 5, 1), (5, 5, 1), (11.25, 2, 1.1), (11.25, 2, 1.2), (3.75, 10, 2.5). Dashed black line: Theory (Eq. (10)) The inset shows a blowup of the same data. After Ref. [23].

are monovalent, and the system as a whole is electroneutral. Charged particles interact with each other *via* a Coulomb potential with the Bjerrum length $\lambda_B = e^2/4\pi\epsilon_r k_B T = 1.0\sigma$, and also with an external electric field $E_x = -1.0\epsilon/\sigma$. Specifically, we show here results for systems with channel width 8σ and a surface charge density $\sigma_A = -0.208e\sigma^{-2}$, which is found to correspond to the 'weak-coupling regime' [16], *i.e.*, the regime where the Poisson-Boltzmann theory is valid. The total counterion density was roughly $\rho_{\text{counter}} = 0.06\sigma^{-3}$ and the salt density varied between $\rho_s = 0.05625, 0.0375, 0.03, 0.025, \text{ and } 0.015\sigma^{-3}$. In molar units, this corresponds to 0.272, 0.181, 0.145, 0.121 and 0.072 mol/l, if we identify $\lambda_B \approx 0.7$ nm, *i.e.*, the Bjerrum length in water at room temperature [3].

3.2. Tunable Slip boundaries

To realize arbitrary hydrodynamic boundary condition at the walls, we introduce an additional coordinate-dependent viscous force that mimicks a wall/fluid friction [23]

$$\vec{F}_i^L = \vec{F}_i^D + \vec{F}_i^R \quad (7)$$

with a dissipative contribution

$$\vec{F}_i^D = -\gamma_L \omega_L(z) (\vec{v}_i - \vec{v}_{\text{wall}}) \quad (8)$$

coupling to the relative velocity $(\vec{v}_i - \vec{v}_{\text{wall}})$ of the particle with respect to the wall, and a stochastic force

$$F_{i,\beta}^R = \sqrt{2\gamma_L k_B T \omega_L(z)} \chi_{i,\beta}. \quad (9)$$

Here β runs over $\beta = x, y, z$, $\chi_{i,\beta}$ is a Gaussian distributed random variable with mean zero and unit variance, and

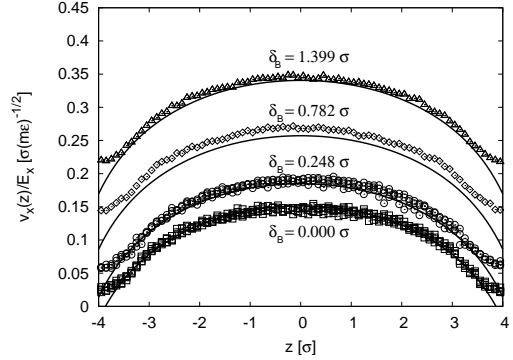


Figure 2: Flow profiles for counterion-induced flow at field strengths $E_x = 0.8 - 1.0k_B T/e\sigma$ for varying slip lengths in the weak coupling regime. The straight lines represent the theoretical prediction of Eqn.(11).

the weight function $\omega_L(z)$ is chosen $\omega_L(z) = 1 - z/z_c$ up to a cut-off distance z_c . The prefactor γ_L sets the strength of the friction force and hence determines the value of the slip length. With this approach it is possible to tune the slip length δ_B systematically from full-slip to no-slip and even (small) negative slip. Furthermore, one can use the Stokes equation to derive an analytical expression for the slip length δ_B as a function of the model parameters, giving [23]

$$\frac{\delta_B}{z_c} = -1 + \frac{1}{(3\alpha)^{1/3}} \frac{\Gamma\left(\frac{1}{3}\right)}{\Gamma\left(\frac{2}{3}\right)} \frac{I_{-2/3}\left(\frac{2\sqrt{\alpha}}{3}\right)}{I_{2/3}\left(\frac{2\sqrt{\alpha}}{3}\right)} \quad (10)$$

where Γ is the Gamma-Function, I the modified Bessel function of the first kind, and the dimensionless parameter $\alpha = z_c^2 \gamma_L \rho / \eta_s$ depends on the density ρ and the shear viscosity η_s of the fluid. To test this expression, we have studied driven neutral fluids in our slit channels for the range of parameters $\gamma_L = (0.1 - 5) \sqrt{m\epsilon}/\sigma$, $\rho = (3.75 - 12.5) \sigma^{-3}$, and $\gamma_{DPD} = (1 - 10) \sqrt{m\epsilon}/\sigma$. By performing Plane Poiseuille and Plane Couette flow simulations, one can determine η_s , δ_B , and the position of the hydrodynamic boundary independently [23]. As expected, the hydrodynamic boundary is always close to the physical boundary, whereas the slip length varies over a wide range. Fig. 1 shows that the results agree very nicely with the theoretical prediction, Eq. (10) [23].

4. Results

4.1. Counterion-induced electroosmotic flow

We begin with discussing the "simpler" situation without polyelectrolyte and salt, where the fluid only

contains the counterions of the charges in the wall. In the regime of validity of the Poisson-Boltzmann equation (the weak coupling limit) the potential distribution $\psi(z)$ can be calculated analytically, giving [1] $\psi(z) \propto \log(\cos^2(\kappa_c z))$, which results in the counterion distribution $\rho_c(z) = \rho_0 / \cos^2(\kappa_c z)$ with the screening constant $\kappa_c^2 = e^2 \rho_0 / 2\epsilon_r \epsilon_0 k_B T$. The parameter ρ_0 (the counterion density in the middle of the channel) is set by the electroneutrality requirement, *i.e.*, the integrated counterion density $\int dz \rho_c(z)$ must equal the surface charge density σ_A . In our case, the corresponding calculation gives $\rho_0 = 0.0174\sigma^{-3}$, in accordance with the numerical value, $\rho_0 = (0.0176 \pm 0.0001)\sigma^{-3}$ [16]. By virtue of Eq. (1) combined with (2), one finally obtains the explicit expression

$$v_x(z) = \frac{e}{4\pi\lambda_B Z \eta_s} E_x \left(\log \left(\frac{\cos^2(\kappa_c z_B)}{\cos^2(\kappa_c z)} \right) + 2\kappa_c \delta_B \tan(\kappa_c z_B) \right) \quad (11)$$

for the flow profile, where we have expressed ϵ_r in terms of the Bjerrum length λ_B . Fig. 2 compares our numerical results for varying surface characteristics (slip lengths) and field amplitudes with the theoretical prediction, Eq. (11). The theory describes the data very nicely, without any fit parameter.

4.2. The full problem

We are now ready to consider the full problem, *i.e.*, a system containing polyelectrolyte, counterions, and varying amounts of salt ions, $\rho_s = 0.015 - 0.056\sigma^{-3}$.

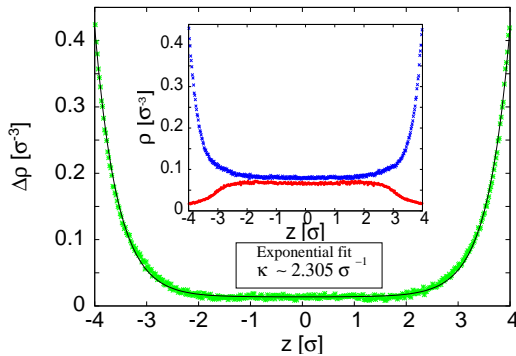


Figure 3: **Inset:** Distribution ρ_c of cations (salt cations and counterions, blue symbols) and anions ρ_a (salt anions, red symbols) for a system containing polyelectrolyte at the salt concentration $\rho_s = 0.05625\sigma^{-3}$. **Main frame:** Corresponding ionic difference profile $\Delta\rho = \rho_c - \rho_a$. The exponential fit (black line), gives the effective inverse screening length $\kappa = 2.305 \pm 0.025\sigma^{-1}$.

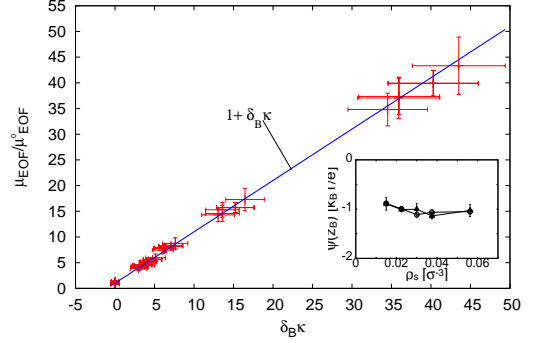


Figure 4: Ratio $\mu_{EOF}/\mu_{0,EOF}$ plotted against $\delta_B\kappa$ for salt concentrations ρ_s ranging in $0.015 - 0.056\sigma^{-3}$ and various slip lengths. The blue line is the theoretical prediction of Eq. (3) with slope $1 + \delta_B\kappa$. **Inset:** Surface potential $\psi(z_B)$ as a function of salt concentration ρ_s .

Fig. 3 shows the ion distribution profiles for one salt concentration. The profiles of the ionic difference exhibit an exponential behavior $f(z) = A(e^{-\kappa z} + e^{\kappa z} + c)$, although the fitted screening parameter $\kappa = (2.305 \pm 0.025)\sigma^{-1}$ does not agree well with the Debye-Hückel screening length, $\kappa_D = 1.21\sigma^{-1}$. Similar observations were made at all other salt concentrations: For the surface charge $\sigma_s = 0.208\sigma^{-2}$, the linearized Debye-Hückel theory is not valid. Nevertheless, a well-defined surface screening length κ can be extracted from the data by a simple exponential fit.

Next we discuss the electroosmotic flow in these channels. Fig. 4 compiles our numerical results for the EOF mobility for all salt concentrations and slip lengths. They are in very good agreement with the theoretical prediction of Eq. (3), where μ_{EOF}^0 has been determined independently by a linear regression for each salt concentration. It is worth noting that the presence of the polyelectrolyte does not perturb the amplitude of the electroosmotic flow.

Finally, we consider the effective migration of the polyelectrolyte in the electric field. It results from a combination of two effects: the 'bare' electrophoresis relative to the surrounding fluid, and the convective transport by the electroosmotic flow. In many situations of interest, one can argue that these two contributions simply add up [14, 17]. The total mobility μ_t is then given by $\mu_t = \mu_{EOF} + \mu_e$, where μ_e is the electrophoretic mobility of the polyelectrolyte in a hypothetical fluid at rest, and by virtue of Eq. (3), it can be expressed in terms of the electroosmotic mobility μ_{EOF} as

$$\frac{\mu_t}{\mu_{EOF}} = 1 + \frac{\mu_e}{\mu_{EOF}^0 (1 + \kappa \delta_B)}, \quad (12)$$

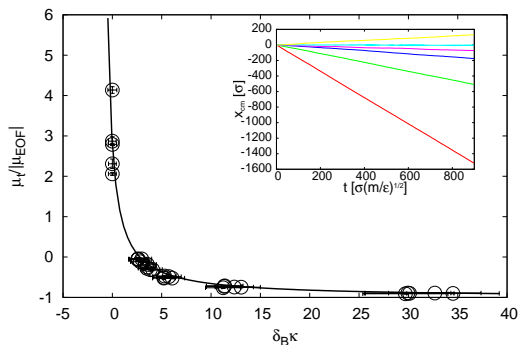


Figure 5: Ratio μ_t/μ_{EOF} plotted against $\delta_B \kappa$ for all salt concentrations. The black line is the theoretical prediction of Eq. (12), with one single fit parameter $\mu_e/\mu_{EOF}^0 = -3.778 \pm 0.128$. Negative values of μ_t/μ_{EOF} indicate absolute negative total mobilities of the polyelectrolyte. **Inset:** Total displacement of the polyelectrolytes center of mass for different boundary conditions at the salt concentration $\rho_s = 0.05625\sigma^{-3}$. The lines correspond from top to bottom to the slip lengths $\delta_B \approx (0.00, 1.292, 1.765, 2.626, 5.664, 14.98)\sigma$.

where the ratio μ_e/μ_{EOF}^0 is expected to depend only weakly on the ionic strength of the electrolyte and the slip length of the surface. The main effect of slippage is incorporated in the factor $(1 + \kappa \delta_B)^{-1}$ [17].

Our numerical results for the total mobility of the polyelectrolyte for varying boundary conditions are presented in Fig. 5. They are in excellent agreement with the theoretical prediction, Eq. (12), with one single fitted ratio $\mu_e/\mu_{EOF}^0 = -3.778 \pm 0.128$. For stick boundaries ($\delta_B \approx 0$) one obtains ordinary behaviour where the polyelectrolyte follows the electric force acting on the monomers. In the presence of slip, the absolute mobility may become negative if the electroosmotic flow exceeds a critical value. This is because the immobile wall charges and the charges on the polyelectrolyte have the same sign, hence the directions of the EOF and the bare electrophoresis are opposite. If the wall charges and the polyelectrolyte charges are opposite, slippage effects should enhance the total mobility of the polyelectrolyte.

5. Conclusions and Outlook

We have presented mesoscopic DPD simulations of EOF and polyelectrolyte electrophoresis in narrow microchannels, taking full account of hydrodynamic and electrostatic interactions. Slippage effects massively influence the electroosmotic flow and therefore the total mobility of the polyelectrolyte. Under certain conditions, even a negative mobility can be achieved, in

agreement with recent experiments [13]. All our numerical results are in good agreement with analytical expressions, which were derived based on the Stokes equation.

In sum, our mesoscopic simulations indicate that the migration of polyelectrolytes in nanochannels results from the interplay of electroosmotic, electrophoretic, electrostatic and slippage effects. To describe the mobility adequately, all of these factors need to be accounted for. From a technological point, the characteristics of the channel walls could be used to significantly enhance flow amplitudes, which offers the possibility to reduce the time needed for polymer migration or separation techniques. This could be an important aspect for future applications in microchannels or micropumps.

Acknowledgment We have benefitted from interactions and discussions with Michael P. Allen, Christian Holm, Burkhard Dünweg, Ulf D. Schiller, Marcello Sega, and Kai Grass. The simulations were carried out at the Arminius Cluster PC² at Paderborn University, the HLRS in Stuttgart and the NIC computing center in Jülich for computer time. This work was funded by the Volkswagenstiftung.

References

- [1] Israelachvili, J.: Intermolecular and Surface Forces. Academic Press, London (1991).
- [2] Hunter, R. J.: Foundations of Colloid Science, Vol.1. Clarendon Press, Oxford (1991).
- [3] Viovy, J.-L.: Rev. Mod. Phys. **72**, 813 (2000).
- [4] Iki, N.; Kim, Y.; Yeung, E. S.: Anal. Chem. **68**, 4321 (1996).
- [5] Roeraade, M.; Stjernström, M. International Patent WO/1997/26531, **1997**, available at <http://www.wipo.int>.
- [6] Effenhauser, C. S.; Bruin, G. J. M.; Paulus, A.: Electrophoresis **18**, 2203 (1997).
- [7] Bader, J. S. *et al*: PNAS **96**, 13165 (1999).
- [8] Han, J.; Craighead, G.: Science **288**, 1026 (2000).
- [9] Han, J.; Turner, S. W.; Craighead, G.: Phys. Rev. Lett. **83**, 1688 (2002).
- [10] Huang, L. R. *et al*: Nature Biotechnology **20**, 1048 (2002).
- [11] Duong, T. T. *et al*: Microelectronic Engineering **67**, 905 (2003).
- [12] Ros, A. *et al*: J. Biotechnology **112**, 65 (2004).
- [13] Mathe, J., Di Meglio, J. -M., Tinland, B.: J. Colloid Interface Sci., **316**, 831 (2007).
- [14] Streek, M. *et al*: J. Biotechnology **112**, 79 (2004).
- [15] Streek, M. *et al*: Phys. Rev. E **71**, 11905 (2005).
- [16] Smiatek, J. *et al*: J. Chem. Phys. **24**, 244702 (2009).
- [17] Smiatek, J., Schmid, F.: J. Phys. Chem. B. **114**, 6266 (2010)
- [18] Hoogerbrugge, P. J., Koelman, J. M. V. A.: Europhys. Lett. **19**, 155, (1992).
- [19] Español, P., Warren, P. B.: Europhys. Lett. **30**, 191 (1995)
- [20] Joly, L. *et al*: Phys. Rev. Lett. **93**, 257805 (2004).
- [21] Arnold, A. *et al*, Comp. Phys. Comm., **174**, 704 (2005).
- [22] Weeks, J. D.; Chandler, D.; Andersen, H. C.: J. Chem. Phys. **54**, 5237 (1971).
- [23] Smiatek, J., Allen, M. P., Schmid, F.: Eur. Phys. J. E, **26**, 115 (2008).